Quantum interference corrections to magnetoconductivity in graphene

S. Pezzini,[1,2] C. Cobaleda,[2] E. Diez,[2] and V. Bellani[1]
[1]*Dipartimento di Fisica and CNISM, Università degli studi di Pavia, I-27100 Pavia, Italy*
[2]*Laboratorio de Bajas Temperaturas, Universidad de Salamanca, E-37008 Salamanca, Spain*
(Received 17 January 2012; revised manuscript received 4 April 2012; published 30 April 2012)

We studied *weak localization* (WL) and *antilocalization* (WAL) in graphene at temperatures between 0.3 K and 15 K. At low carrier density, we observed a transition from WL to WAL driven by the increasing of the magnetic field while at high carrier density, WAL was suppressed as a consequence of trigonal warping of the conical energy bands. We analyzed the magnetic-field-driven WL-WAL transition, evaluating the relative strengths of the various elastic-scattering mechanisms and estimating the decoherence lengths (l_ϕ) and rates (τ_ϕ^{-1}) as a function of temperature, using an alternative method with respect to previously reported studies. We relate the small values of l_ϕ here reported, confirmed by a complementary analysis of universal conductance fluctuations, to an effective breaking of time-reversal symmetry due to the slowly varying disorder of the long-range type.

DOI: 10.1103/PhysRevB.85.165451 PACS number(s): 73.43.Qt, 72.80.Vp, 72.15.Rn

Quantum interference strongly affects the conduction properties of two-dimensional systems at very low temperatures,[1] inducing measurable deviations from the predictions of Drude's semiclassical model[2] (electrical conductivity $\sigma_0 = n\mu e$, where n is the charge-carrier density and μ is the charge-carrier mobility). In particular, the constructive interference between time-reversed counter-propagating closed electronic paths [Fig. 1(a)] enhances the back-scattering probability, lowering the effective value of conductivity with respect to σ_0. This effect is known as *weak localization* (WL).[3] Such a constructive quantum interference takes place as far as charge carriers keep their phase coherence during their motion, and time-reversal symmetry holds. The loss of phase coherence induced by inelastic scattering can be taken into account, introducing a *decoherence length* l_ϕ (and a related *decoherence time* τ_ϕ) that limits the number of constructively interfering paths to that of length $L < l_\phi$ (covered in a time $t < \tau_\phi$). This argument leads to a zero-field WL correction of the conductivity[1]

$$\delta\sigma_{\mathrm{WL}} = g_s g_v \frac{e^2}{4\pi^2\hbar} \ln\left(1 + \frac{\tau_\phi}{\tau}\right), \qquad (1)$$

where g_s and g_v are the spin and valley degeneracies, respectively, ($g_s = g_v = 2$ in graphene[4]) and τ is the mean elastic-scattering time, the ratio of which with τ_ϕ essentially determines the $\delta\sigma_{\mathrm{WL}}$ amplitude. Time-reversal symmetry is broken by the application of a magnetic field perpendicular to the two-dimensional electron gas. The development of Aharonov-Bohm phases[5] $\delta\varphi \approx \pi\frac{\phi}{\phi_0}$ ($\phi = BS$ is the magnetic flux winded by a trajectory of enclosed area S while $\phi_0 = h/e$ is the magnetic flux quantum) between time-reversed paths lowers the number of constructive-interference events so that σ_0 tends to be restored in a finite magnetic field. This fact can be taken into account by introducing a characteristic *magnetic length* $l_m = (\hbar/eB)^{\frac{1}{2}}$ (*magnetic time* $\tau_B = l_m^2/2D$, where D is the diffusion coefficient), which restricts the contribution to WL to those loops enclosing an area $S < {l_m}^2$ (covered in a time $t < \tau_B$). Therefore, the magnetoconductivity is expected to be characterized by a minimum at $B = 0$ and a subsequent growth at increasing B.

The peculiar electronic properties of graphene[6–8] are expected to give rise to anomalous quantum-interference behaviors. Charge carriers in graphene are indeed of chiral nature, i.e., the electronic states of the Dirac-like Hamiltonian $H_{\mathbf{K}} = v_f\boldsymbol{\sigma}\cdot\mathbf{p}$ ($v_f \simeq 10^6$ m/s is the Fermi velocity of electrons in graphene and $\mathbf{p}$ is the momentum operator while $\boldsymbol{\sigma}$ is the *pseudospin* operator) have to be simultaneous eigenstates of the helicity operator $h = \frac{\boldsymbol{\sigma}\cdot\mathbf{p}}{|\mathbf{p}|}$ with well-defined conserved eigenvalues: $+1$ for electrons in the $\mathbf{K}$ valley (holes in the $\mathbf{K}$' valley) and -1 for electrons at $\mathbf{K}$' (holes at $\mathbf{K}$) [see Fig. 1(b)]. A backscattering event in real space corresponds to a wave-vector shift $\mathbf{q} \rightarrow -\mathbf{q}$ in reciprocal space, which is prohibited by chirality conservation within a unique valley (*intravalley* event). This fact can be alternatively explained considering that the nontrivial π Berry phase leads to destructive quantum interference between time-reversed closed electronic loops. A zero backscattering probability, i.e., chiral charges performing the so-called *Klein tunneling* paradox,[9,10] implies an increased conductivity with respect to σ_0. This is the so-called *weak antilocalization* (WAL) effect, which has already been studied in materials characterized by strong spin-orbit coupling.[11] In an analogous way to WL, WAL manifests itself as a maximum in the conductivity at zero B, which decreases at increasing magnetic fields.

Other mechanisms have to be taken into account in order to understand the magnetoconductivity in graphene. First of all, far away from the degeneracy points $\mathbf{K}$ and $\mathbf{K}$', the energy bands of graphene deviate from a perfect conical shape (*trigonal warping*) so that chirality ceases to be a good quantum number. This allows intravalley-backscattering events which reduce and progressively suppress WAL. Moreover, since charge carriers have opposite chirality at $\mathbf{K}$ and $\mathbf{K}$', *intervalley*-backscattering events conserve chirality. Therefore, backscattering is allowed in graphene as in an ordinary conductor so that, in the presence of intervalley scattering (induced by very short-range potentials such as single-vacancy scatterers[12]), WL is expected to emerge.

We can associate the mean elastic-scattering time τ_s to the intravalley events for which chirality is a good quantum number, τ_w to the intravalley events without chirality conservation, and τ_i to the intervalley events. The relative strength of these

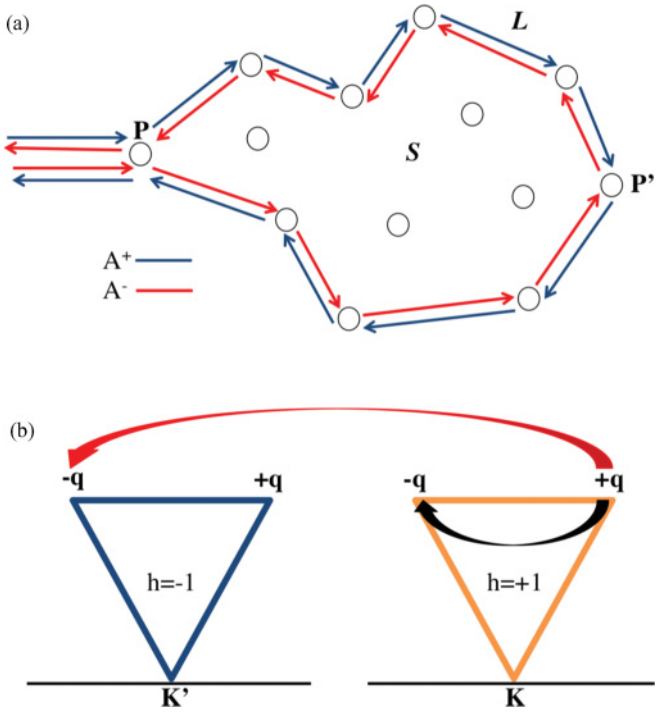

FIG. 1. (Color online) (a) Schematic picture of two closed PP'P electronic paths (for which interference gives rise to WL, see text) of length L, including an area S. A probability amplitude $A^+ = ae^{i\varphi^+}$ ($A^- = ae^{i\varphi^-}$) is associated with the clockwise (counterclockwise) trajectory. The backscattering probability is obtained by applying the superposition principle $p = |A^+ + A^-|^2 = 2a^2 + 2a^2e^{i(\varphi^+ - \varphi^-)}$; it exactly doubles the classical value in the case of constructive interference. (b) Pictorial view of intravalley (black arrow) and intervalley (red arrow) backscattering events in graphene's reciprocal space.

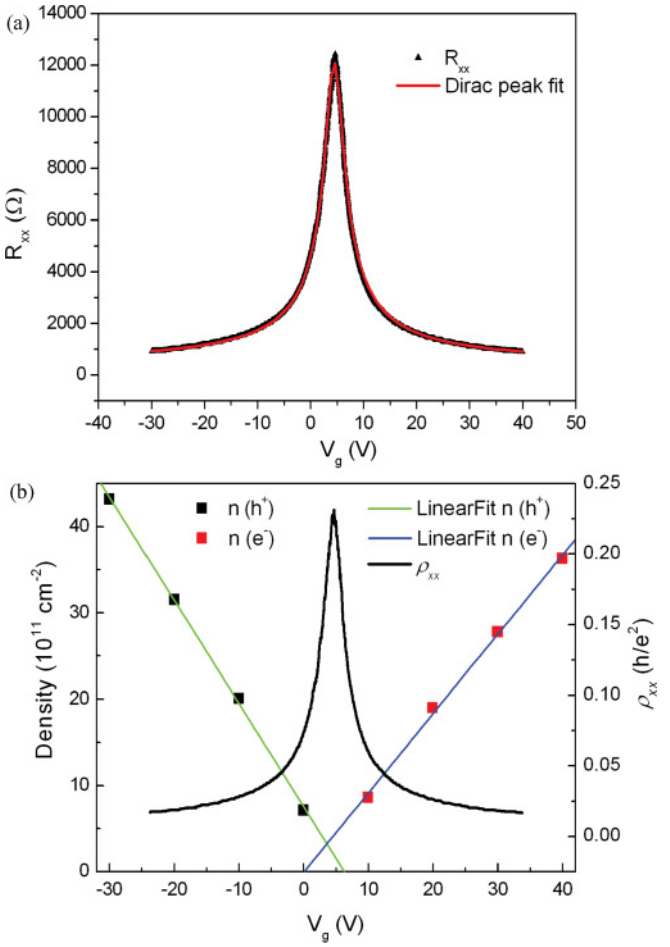

FIG. 2. (Color online) (a) Longitudinal resistance as a function of gate voltage (V_g), fitted with the procedure described in Ref. 17 (red). (b) Charge-carrier density as a function of V_g both in the electron and hole regimes.

parameters determines the WL-WAL behavior experimentally observable.

The first experimental studies on graphene did not show clear evidence of WL.[13] Later, the fabrication of samples with higher mobility has allowed the clear observation of WL[14] and WAL[15] in magnetotransport measurements with a strong dependence on physical parameters like temperature and charge density. From a theoretical point of view, a complete expression of the WL correction to the magnetoconductivity in graphene was derived by McCann *et al.*[16] Here, we report on the magnetotransport measurements performed on exfoliated graphene, which evidence both WL and WAL. The evolution of magnetoconductivity with temperature has been studied for different values of charge density. Making use of an alternative method with respect to the usual analysis (which is based on the function developed by McCann *et al.*), we were able to estimate the decoherence lengths and rates relative to different charge densities and their temperature dependences. The method we developed takes advantage of straightforward mathematical relations [see Eqs. (3) and (4)] and permits an intuitive estimation of the relative strengths of the various scattering mechanisms that are present in disordered graphene.

The studied sample is a monolayer-graphene Hall bar with dimensions $W \times L = 5.1\ \mu\text{m} \times 10.6\ \mu\text{m}$, giving a geometrical factor $W/L \simeq 0.5$. It was produced by mechanical exfoliation (*scotch-tape technique*), placed on the top of a Si/SiO_2 substrate (with a SiO_2 thickness of 300 nm) and processed by means of e-beam lithography (50/500 Å thick Ti/Au ohmic contacts). The longitudinal (R_{xx}) and Hall (R_{xy}) resistances were measured with the standard ac lock-in technique, applying a longitudinal current of intensity $1\ \text{nA} < i < 10\ \text{nA}$ at frequency $10\ \text{Hz} < f < 15\ \text{Hz}$. The sample was placed in a cryogen-free ^{3}He refrigerator with a base temperature $\simeq$0.3 K, located in the room-temperature access bore of an also cryogen-free superconducting magnet.

In order to preliminarily characterize the sample, we performed zero-field measurements of R_{xx} as a function of back-gate potential (V_g) at $T = 0.3$ K. From the measured data we extracted the plot of the so-called *Dirac peak* of the sample (see Fig. 2). We performed a fit of the Dirac peak following the procedure described by Kim *et al.*,[17] obtaining the position of the charge-neutrality point at $V_D \simeq 4.66$ V and the residual charge density $n_{\text{res}} \simeq 2 \times 10^{11}\ \text{cm}^{-2}$. Using the relation $n_{\text{res}} \simeq 0.2 \times n_{\text{imp}}$,[18] we estimated the impurities' concentration at the SiO_2-graphene interface $n_{\text{imp}} \simeq 10^{12}\ \text{cm}^{-2}$. These values clearly indicate that a dirt-graphene sample for which electric transport is diffusive rather than ballistic was studied. Assuming a uniform distribution, the mean separation

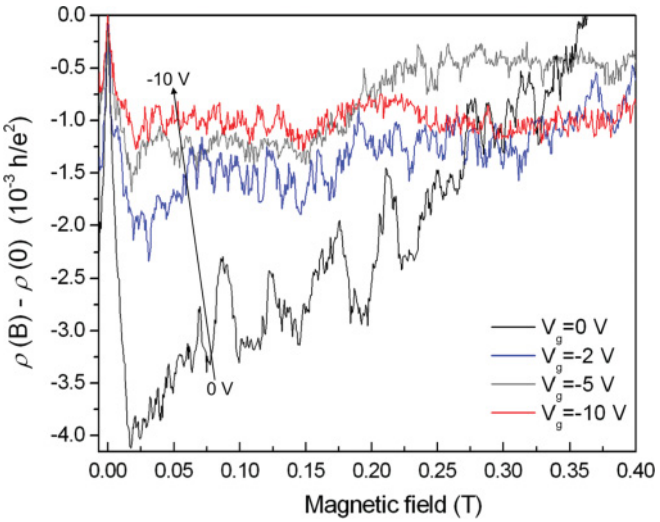

FIG. 3. (Color online) WL-WAL corrections to the magnetoresistivity for different V_g values (ranging from 0 V to −10 V) at $T = 0.3$ K. One can note the strong presence of universal conductance fluctuations in the data collected.

between the interface impurities results in $l \simeq 10$ nm, which is two orders of magnitude larger than the nearest-neighbor distance $a = 1.42$ Å. The condition $l \gg a$ implies that the charged impurities at the SiO_2-graphene interface produce a slowly varying potential of the long-range type, which influence on quantum-interference events will be taken into account.

We successively measured the Hall resistance $R_{xy}(B)$ in the hole region ($V_g < V_D$) at $T = 0.3$ K in order to evaluate both the bidimensional charge-carrier density n and the mobility μ. These quantities have been calculated using the standard formulas $n = 1/(es)$ and $\mu = 1/(ne\rho^0_{xx})$, where $s = dR_{xy}/dB$ was obtained from a linear fit of $R_{xy}(B)$ while ρ^0_{xx} was the longitudinal resistivity at $B = 0$. At $V_g = 0$ V and $V_g = -10$ V (values selected for the successive WL-WAL studies), we obtained $n(0\text{ V}) = 7 \times 10^{11}$ cm^{-2} and $\mu(0\text{ V}) = 4038$ cm^2 V^{-1} s^{-1} and $n(-10\text{ V}) = 2 \times 10^{12}$ cm^{-2} and $\mu(-10\text{ V}) = 3657$ cm^2 V^{-1} s^{-1}, respectively. From these values, we, therefore, calculated the Drude conductivities $\sigma_0(0\text{ V}) = 11.9\, e^2/h$ and $\sigma_0(-10\text{ V}) = 30.2\, e^2/h$.

The first objective of our WL study was to characterize the magnetotransport behavior of the sample tuning the gate potential. In Fig. 3 one can clearly see two effects. The first one, observable at magnetic fields close to zero, consists of a decrease of the WL peak's height with increasing V_g. The gate potential drives the Fermi level far from the charge-neutrality point, adding charge carriers to the sample. Accordingly, the hole-hole-scattering rate is increased, and therefore, τ_ϕ decreases so that the number of constructively interfering closed paths that contribute to the enhancement of the backscattering probability is lowered. Furthermore, looking at the whole B range, we can see that, besides the WL peak, the data also show evidence of WAL (increasing magnetoresistivity with increasing B). This is noticeable at $V_g = 0$ V (black line) while it tends to disappear with an increasing gate potential (blue and gray lines) and is absent at $V_g = -10$ V (red line). This is in agreement with the fact that as the Fermi level is driven far from the band-degeneracy points, the trigonal-warping effect suppresses the chirality conservation and, accordingly, the WAL effect. Therefore, the sample is switched from a regime where $\tau_s^{-1} > \tau_w^{-1}$ ($V_g = 0$ V, intravalley scattering unaffected by the trigonal warping) to a trigonal-warping-dominated regime ($V_g = -10$ V) where $\tau_s^{-1} < \tau_w^{-1}$.

Our data indicate that chirality is a good symmetry at least in the proximity of the charge-neutrality point. Chirality-breaking events with origins different from trigonal warping (induced for instance by dislocations and ripples in the graphene structure) are assumed to be negligible in the sense that they do not prevent WAL to manifest, and the suppression of WAL with increasing gate voltage is clearly due to warping of the conical-band structure.

The following objective was the study of the effect of temperature on the WL corrections to the magnetoconductivity in these two regimes. For this purpose we calculated the longitudinal conductivity using the expression

$$\sigma_{xx} = \frac{\rho_{xx}}{\rho_{xx}^2 + \rho_{xy}^2}. \tag{2}$$

Figure 4 shows σ_{xx} for $V_g = 0$ V [Fig. 4(a)] and $V_g = -10$ V [Fig. 4(b)]. We can clearly see that at all temperatures σ_{xx} presents a hollow around $B = 0$, whose depth decreases with increasing T, since the quantum-interference corrections are suppressed as a consequence of the reduction of the carriers' phase coherence. At low carrier density ($V_g = 0$ V, $n = 7 \times 10^{11}$ cm^{-2}), we again observe evidence of WAL (decreasing magnetoconductivity with increasing magnetic field) while it is not present at higher concentrations ($V_g = -10$ V, $n = 2 \times 10^{12}$ cm^{-2}). At $V_g = 0$ the magnetoconductivity firstly increases and then decreases with increasing B (i.e., with decreasing magnetic time τ_B), showing a maximum at $B \simeq 0.06$ T, both for positive and negative directions of the magnetic field. This is a clear sign of a transition from WL to WAL. Theoretically, this maximum is expected at a characteristic magnetic field B_i at which $\tau_B \approx \tau_i$.[16] From $B_i \simeq 0.06$ T, we can thus estimate the intervalley-scattering rate $\tau_i^{-1} \simeq 3.64 \times 10^{12}$ s^{-1}. From Fig. 4(a) one can see that the value B_i which corresponds to the conductivity maximum (and, consequently, the calculated τ_i^{-1}) is in the first approximation independent of temperature. As the intravalley-scattering-induced WAL survives at fields much higher than B_i (i.e., lower time scales), we argue that $\tau_s^{-1} \gg \tau_i^{-1}$, namely, that the intravalley-long-range-scattering centers (such as charged impurities) dominate over short-range intervalley ones in our sample.

An analogous analysis can be done for the data measured at $V_g = -10$ V, the characteristic magnetic field B_i at which $\tau_B \approx \tau_i$ marks the suppression of WL. We estimated $B_i \simeq 0.02$ T (as one can see in Fig. 4(b), for $B > B_i$ only universal conductance fluctuations (UCF) are observable), giving $\tau_i^{-1} \simeq 2.18 \times 10^{12}$ s^{-1}. We believe that the intervalley-scattering rate is lowered as a consequence of the increasing of Coulomb screening on the short-range-scattering centers for $n = 2 \times 10^{12}$ cm^{-2}.

Considering that in graphene only intervalley-scattering processes contribute to WL, we adapted Eq. (1) to the

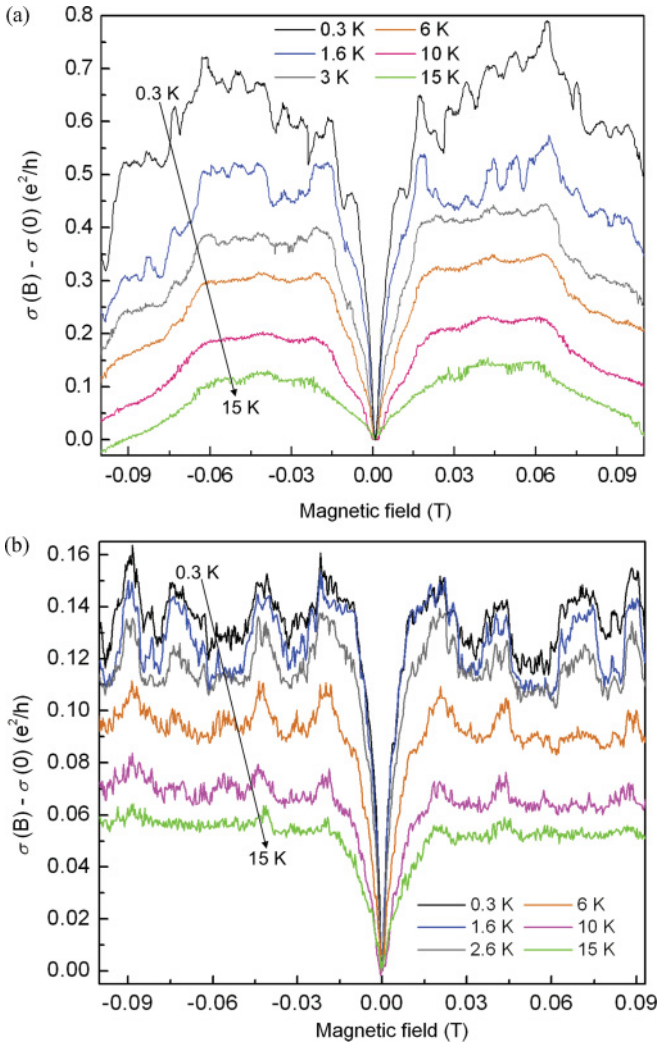

FIG. 4. (Color online) Temperature evolution of WL-WAL corrections to the magnetoconductivity at (a) $V_g = 0$ V and (b) $V_g = -10$ V for 0.3 K $< T <$ 15 K.

graphene's case, so we can write

$$\delta\sigma_{\mathrm{WL}}^{(\mathrm{Graphene})}\left(\frac{e^2}{h}\right) = -\frac{2}{\pi}\ln\left(1+\frac{\tau_\phi}{\tau_i}\right). \tag{3}$$

From this expression we can easily estimate the decoherence time τ_ϕ (and the related parameters) from the peak-to-valley value of the WL-conductivity dips $\delta\sigma$ of Fig. 4 by means of the relation

$$\tau_\phi = \left(e^{\delta\sigma\frac{\pi}{2}} - 1\right)\tau_i. \tag{4}$$

Figure 5 shows the temperature dependence of the decoherence rates and lengths for the two regimes considered. In the inset we can see that the phase-breaking rate τ_ϕ^{-1} grows linearly with temperature (note the linear fits) and that in the high-density regime it has higher values and increases more rapidly than in the low-density regime. The resulting $\mathrm{T}^{-1/2}$ dependence of $l_\phi = (D\tau_\phi)^{1/2}$ is in accordance with the relation $l_\phi \approx (E_f/2KT)^{1/2}$ (Ref. 13) and indicates that the carrier-carrier Coulomb interaction is the dominant dephasing mechanism.

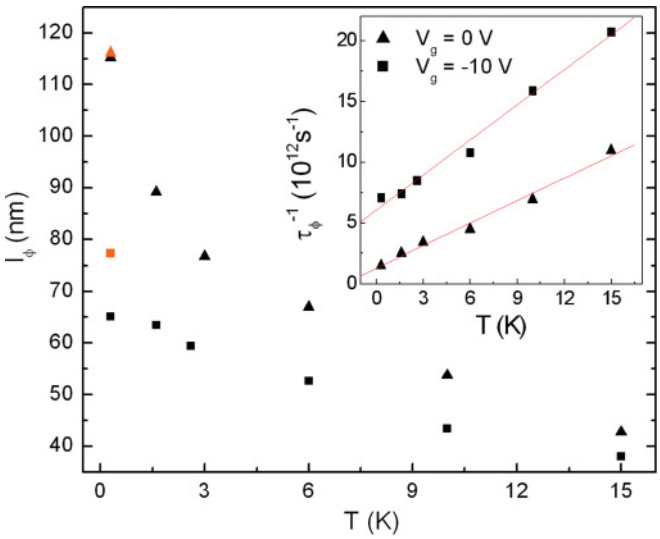

FIG. 5. (Color online) Temperature dependences of decoherence length and rate (inset), obtained from Eq. (4) for the two density regimes corresponding to $V_g = 0$ V ($n = 7 \times 10^{11}$ cm^{-2}) and $V_g = -10$ V ($n = 2 \times 10^{12}$ cm^{-2}). The orange square and triangle are values obtained from the analysis of the UCF at $T = 0.3$ K. The red lines are linear fits to τ_ϕ^{-1}.

The absolute values of the decoherence lengths showed in Fig. 5 are quite lower with respect to the ones reported in previous studies.[14] A possible explanation can be found considering that dephasing may not be the only origin of the temporal cutoff to the quantum-interference processes. Indeed, we have to take into account that the slowly varying long-range potential produced by the doping impurities at the graphene-SiO_2 interface (with concentration 10^{12} cm^{-2}) effectively breaks the time-reversal symmetry (just like a finite magnetic field would do).[19] This fact implies a decrease of the absolute value of the correction $\delta\sigma_{\mathrm{WL}}$ and, as a consequence of Eqs. (3) and (4), of τ_ϕ (and of the related parameter l_ϕ). Nevertheless, since the impurity-related contribution does not depend on temperature, we can state that the strong temperature dependence shown in Fig. 5 comes from *e-e* dephasing.

In order to verify the reliability of our values, we estimated l_ϕ also with another methodology, based on the analysis of the universal conductance fluctuations. Indeed, we observed highly reproducible quantum fluctuations at the lowest temperatures ($T \leqslant 3$ K, see Fig. 6). Following the argument of Lee *et al.*,[20] we performed a root-mean-square analysis of the data, using the expression

$$[\langle(\sigma - \langle\sigma\rangle)^2\rangle]^{1/2} = \frac{L}{W}\frac{g_s g_v}{2\beta^{1/2}}C\left(\frac{e^2}{h}\right)\left(\frac{l_\phi}{L}\right)^{3/2}. \tag{5}$$

In this analysis we used $\beta = 1$ and $C = \sqrt{12}$ at $T = 0.3$ K, and we have considered the range 0.03 T $< B <$ 0.06 T for the $V_g = 0$ V case and the range 0.03 T $< B <$ 0.09 T for $V_g = -10$ V (i.e., the intervals where the UCF are well resolved). The resulting dephasing lengths are $l_\phi(V_g = 0\ \mathrm{V}) \simeq 117$ nm (orange triangle in Fig. 5) and $l_\phi(V_g = 0\ \mathrm{V}) \simeq 78$ nm (orange square in Fig. 5), which are in a satisfying agreement with the values previously obtained from Eq. (4).

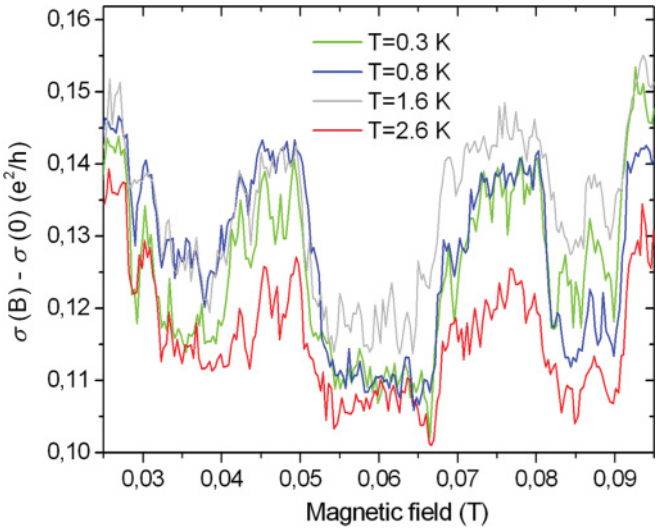

FIG. 6. (Color online) Universal conductance fluctuations for $V_g = -10$ V, measured at different temperatures below 3 K.

In conclusion, we studied the quantum-interference corrections to conductivity at low magnetic fields and low temperatures in mechanically exfoliated monolayer graphene at different charge-carrier densities in the hole region. We found evidence of both WL and WL combined with WAL, depending on the relative strengths of the various elastic-scattering mechanisms, and the results depend on the carrier density. The temperature dependences of the decoherence rate and length have been estimated using an alternative method with respect to previous studies and indicate that the carrier-carrier Coulomb interaction is the main dephasing mechanism in graphene at our densities. The low values reported (corroborated by an analysis of the UCF) have been related to an effective breaking of time-reversal symmetry due to the presence of long-range slowly varying potentials that have been shown to be the dominant disorder. The extreme sensitivities of WL and WAL to various elastic-scattering mechanisms (which is a direct consequence of the unique topology of graphene's bands) hint at the use of magnetotransport measurements as a tool of characterization of both unintentional and intentional disorder in graphene. Thinner conduction channels (that should enhance intervalley-edge scattering), strain-induced defects, and alternative substrates could be the objects of future studies.

We are thankful to David López and Mario Amado and to the ISOM for their help during the sample process. This work has been supported by the following projects: MICINN (Spain) Grants No. FIS2009-07880 and No. PCT310000-2009-3 and Junta de Castilla y León Grant No. SA049A10.

[1]C. W. J. Beenakker and H. van Houten, Solid State Phys. **44**, 1 (1991).
[2]N. W. Ashcroft and N. D. Mermin, *Solid State Physics* (Saunders, Philadelphia, 1976).
[3]G. Bergmann, Phys. Rev. B **28**, 2914 (1983).
[4]K. S. Novoselov, A. K. Geim, S. V. Morozov, D. Jiang, M. I. Katsnelson, I. V. Grigorieva, S. V. Dubonos, and A. A. Firsov, Nature (London) **438**, 197 (2005).
[5]Y. Aharonov and D. Bohm, Phys. Rev. **115**, 485 (1959).
[6]K. S. Novoselov, S. V. Morozov, T. M. G. Mohiuddin, L. A. Ponomarenko, D. C. Elias, R. Yang, I. I. Barbolina, P. Blake, T. J. Booth, D. Jiang, J. Giesbers, E. W. Hill, and A. K. Geim, Phys. Status Solidi B **244**, 4106 (2007).
[7]A. H. Castro Neto, F. Guinea, N. M. R. Peres, K. S. Novoselov, and A. K. Geim, Rev. Mod. Phys. **81**, 109 (2009).
[8]R. N. M. Peres, Rev. Mod. Phys. **82**, 2673 (2010).
[9]O. Klein, Z. Phys. A **53**, 157 (1929).
[10]M. I. Katsnelson, K. S. Novoselov, and A. K. Geim, Nat. Phys. **2**, 620 (2006).
[11]S. Hikami, A. I. Larkin, and Y. Nagaoka, Prog. Theor. Phys. **63**, 707 (1980).
[12]I. Deretzis, G. Fiori, G. Iannaccone, and A. La Magna, Phys. Rev. B **81**, 085427 (2010).
[13]S. V. Morozov, K. S. Novoselov, M. I. Katsnelson, F. Schedin, L. A. Ponomarenko, D. Jiang, and A. K. Geim, Phys. Rev. Lett. **97**, 016801 (2006).
[14]F. V. Tikhonenko, D. W. Horsell, R. V. Gorbachev, and A. K. Savchenko, Phys. Rev. Lett. **100**, 056802 (2008).
[15]F. V. Tikhonenko, A. A. Kozikov, A. K. Savchenko, and R. V. Gorbachev, Phys. Rev. Lett. **103**, 226801 (2009).
[16]E. McCann, K. Kechedzhi, V. I. Fal'ko, H. Suzuura, T. Ando, and B. L. Altshuler, Phys. Rev. Lett. **97**, 146805 (2006).
[17]S. Kim, J. Na, I. Jo, D. Shahrjerdi, L. Colombo, Z. Yao, E. Tutuc, and S. K. Banerjee, Appl. Phys. Lett. **94**, 062107 (2009).
[18]S. Adam, E. H. Hwang, V. M. Galitski, and S. Das Sarma, Proc. Natl. Acad. Sci. USA **104**, 18392 (2007).
[19]A. F. Morpurgo and F. Guinea, Phys. Rev. Lett. **97**, 196804 (2006).
[20]P. A. Lee, A. D. Stone, and H. Fukuyama, Phys. Rev. B **35**, 1039 (1987).